NANO LETTERS

pubs.acs.org/NanoLett Letter

Critical Role of Sc Substitution in Modulating Ferroelectricity in Multiferroic $LuFeO_3$

Shiqing Deng,*[,▽] Jun Li,[▽] Didrik R. Småbråten,[▽] Shoudong Shen, Wenbin Wang, Jun Zhao, Jing Tao, Ulrich Aschauer, Jun Chen, Yimei Zhu,* and Jing Zhu*

Cite This: https://doi.org/10.1021/acs.nanolett.1c02123 Read Online

ACCESS | Metrics & More | Article Recommendations | Supporting Information

ABSTRACT: Understanding how individual dopants or substitutional atoms interact with host lattices enables us to manipulate, control, and improve the functionality of materials. However, because of the intimate coupling among various degrees of freedom in multiferroics, the atomic-scale influence of individual foreign atoms has remained elusive. Here, we unravel the critical roles of individual Sc substitutional atoms in modulating ferroelectricity at the atomic scale of typical multiferroics, $Lu_{1-x}Sc_xFeO_3$, by combining advanced microscopy and theoretical studies. Atomic variations in polar displacement of intriguing topological vortex domains stabilized by Sc substitution are directly correlated with Sc atom-mediated local chemical and electronic fluctuations. The local FeO_5 trimerization magnitude and Lu/Sc−O hybridization strength are found to be significantly reinforced by Sc, clarifying the origin of the strong dependence of improper ferroelectricity on Sc content. This study could pave the way for correlating dopant-regulated atomic-scale local structures with global properties to engineer emergent functionalities of numerous chemically doped functional materials.

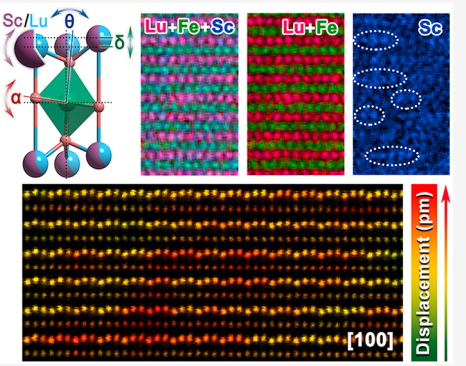

KEYWORDS: *structure−function relationship, individual dopant, multiferroics, lutecium ferrite, improper ferroelectricity, electron microscopy*

Capturing a complete picture of the connection between chemistry, local structure, and functionality is a backbone of solid-state chemistry, which lays the foundation for practical applications and performance control of functional compounds.[1,2] This picture is generally complex and can be much more complicated by doped atoms or chemical substitution, because of the close and intertwined interactions between foreign atoms and host lattices.[3,4] Although it is considerably challenging, bridging such connections in doped or chemically substituted systems by addressing the critical roles of foreign atoms is particularly important and intriguing, into which extensive research endeavor has been continually devoted.[2−6] This is because such foreign atoms can always be the inherent origin of (or the key control parameter for) emergent phenomena or novel functionalities by subtly mediating local crystal, electronic, and defective structures. A typical example includes the giant piezoelectricity recently reported in Sm-doped $Pb(Mg_{1/3}Nb_{2/3})O_3$−$PbTiO_3$ relaxor ferroelectrics, which arises from the enhanced local structural heterogeneity introduced by inhomogeneously distributed Sm dopants.[7] Lacking the in-depth probe of the key behaviors of these dopants or substitutional atoms would lead to an incomplete understanding of the structure−function relationship, preventing us from delving into the underlying chemistry and accurately controlling the materials' functionalities.

As an important branch of the functional compound family, multiferroics, in which ferroelectricity and (anti-)ferromagnetism coexist and are closely coupled, has attracted considerable attention, because of its potential application in the new generation of electronic devices, like ultralow-power information memory.[8,9] Wherein, the intimate coupling among charge, lattice, spin, and orbital degrees of freedom enables the dramatic and effective regulation of multiferroicity by using chemical doping or substitution. For example, in the prototypical room temperature (RT) multiferroic system, $BiFeO_3$, the Ca doping can stimulate an electronic conductor−insulator transition[10] and the La doping can tune the conductivity of the ferroelectric domain wall.[11] However, significant challenges are also introduced at the same time in disentangling the critical effects of these dopants or substitutional elements. In that, the foreign atoms in multiferroics can strongly interact with host lattices with various competing and intertwined degrees of freedom and significantly change the

Received: May 31, 2021
Revised: July 16, 2021

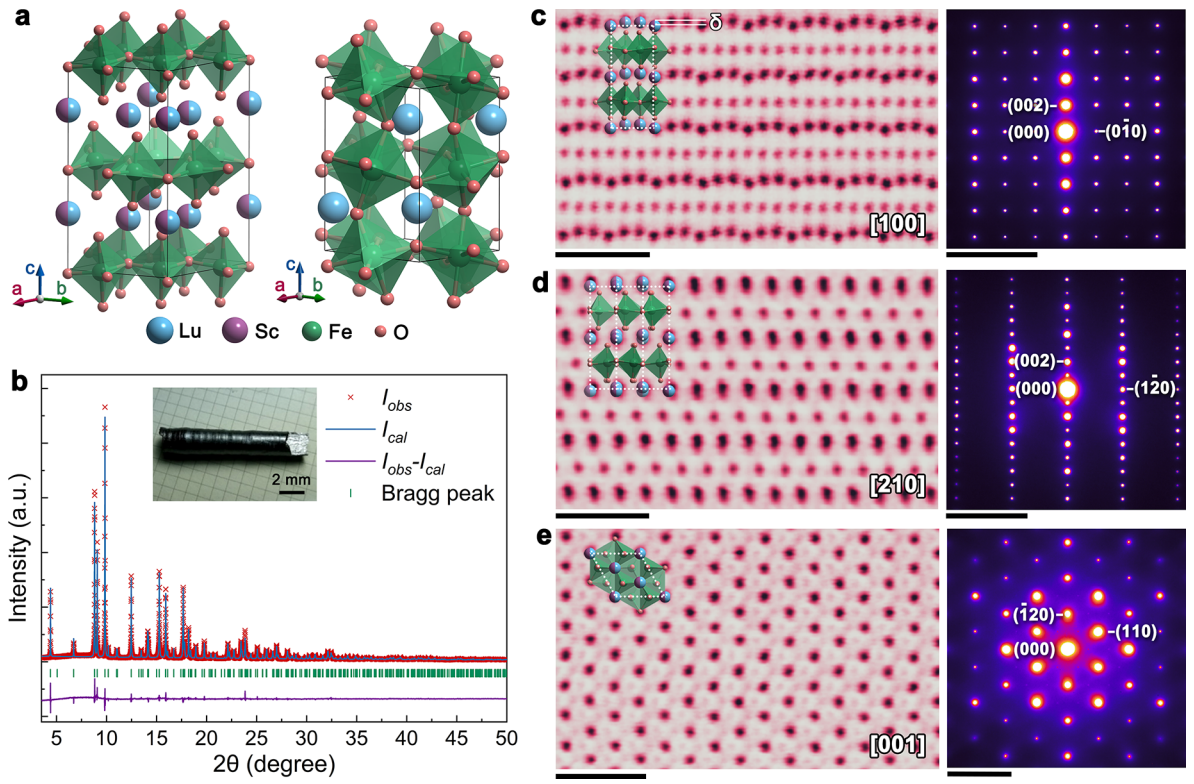

Figure 1. Structural characterization of h-$Lu_{1-x}Sc_xFeO_3$. (a) Crystal structures of h-$Lu_{0.5}Sc_{0.5}FeO_3$ (left) and o-$LuFeO_3$ (right). (b) Rietveld refinement of synchrotron X-ray diffraction (SXRD) results. The difference between the experiment (red cross) and calculation (blue line) is shown at the bottom (purple line). Vertical green lines indicate the Bragg peak positions. (c−e) HAADF-STEM images and corresponding SAED patterns (inset) along three major zone axes. δ represents the **c**-axial displacement. Scale bars are 1 nm for HAADF-STEM images and 5 nm^{-1} for diffraction patterns.

local structures and corresponding electric and magnetic properties.[4,10−12] Therefore, this makes doped or chemically substituted multiferroics quite a challenging but representative system to study, with regard to the critical roles of dopants or substitutional atoms.

Scandium-substituted lutecium ferrite, h-$Lu_{1-x}Sc_xFeO_3$, is a recently developed promising RT multiferroic compound.[12−14] Not only does the robust **c**-axis-oriented ferroelectricity exist well above RT ($T_C \approx 1050$ K), more importantly, it has a much higher antiferromagnetic ordering temperature, because of stronger magnetic interactions between Fe^{3+} spins,[12,15,16] compared to extensively studied isosymmetric manganites (h-$RMnO_3$, R = Ho−Lu, Y, and Sc).[17,18] Wherein, the Sc chemical substitution is well-recognized to be responsible for the significant changes in crystal structure and the emergence of many intriguing properties, like improper ferroelectricity and fascinating topologically protected vortex domain structure, nevertheless, how Sc functions remains elusive.[14,19] In particular, the Sc-substitution-induced vortex domain structure is widely considered to dominate the most desired magnetoelectric (ME) coupling and functional charged domain walls for application in electronic devices, as observed in the hexagonal manganites.[16,20−23] However, to date, only one experimental observation of this vortex domain at the mesoscopic scale was reported in bulk h-$Lu_{1-x}Sc_xFeO_3$.[19] In-depth structural and electronic investigations are still lacking, especially regarding the functionality of Sc substitutional atoms. Note that neither $ScFeO_3$ nor $LuFeO_3$ prefers the hexagonal polar structure,[24−26] and only the solid solution of $ScFeO_3$ (x) and $LuFeO_3$ ($1 - x$) within a certain x range is appropriate for the formation of improper ferroelectricity and vortex domains.[12−14,19,27] The reason for the stabilization of the polar structure and vortex domains by Sc chemical substitution and how Sc atoms modify local structures to regulate the improper ferroelectricity in h-$Lu_{1-x}Sc_xFeO_3$ remain unclear. Thus, it is of great scientific importance to reveal the critical roles of individual Sc substitutional atoms to elucidate the nature of improper ferroelectricity and vortex domains in hexagonal ferrites, and to identify the chemical substitutional atom-tuned couplings among charge, lattice, spin, and orbital degrees of freedom.

In this work, we unravel the critical roles of Sc substitutional atoms in stabilizing the hexagonal polar phase and the vortex domain structure in h-$Lu_{1-x}Sc_xFeO_3$ ($x \approx 0.51$) and directly bridge the individual Sc substitutional atom-mediated local chemical and electronic structures with improper ferroelectricity at the atomic scale. By using advanced scanning transmission electron microscopy (STEM), we quantitatively analyzed the atomic-scale chemistry and ferroelectricity, where the local Sc content fluctuations are found to greatly change the local ferroelectric polarization and can be well-correlated to its variations. The combination of delicate spectroscopy studies with theoretical calculations reveals the origin of this close correlation. It is found that Sc substitutional atoms can modify the local electronic structure and ferroelectric order by changing the magnitude of FeO_5 trimer distortion and the strength of Lu/Sc−O hybridization, which determines the nature of improper ferroelectricity and vortex domain structure. The findings of this work suggest the possibility of tuning and understanding the mechanism of improper

https://doi.org/10.1021/acs.nanolett.1c02123
Nano Lett. XXXX, XXX, XXX−XXX

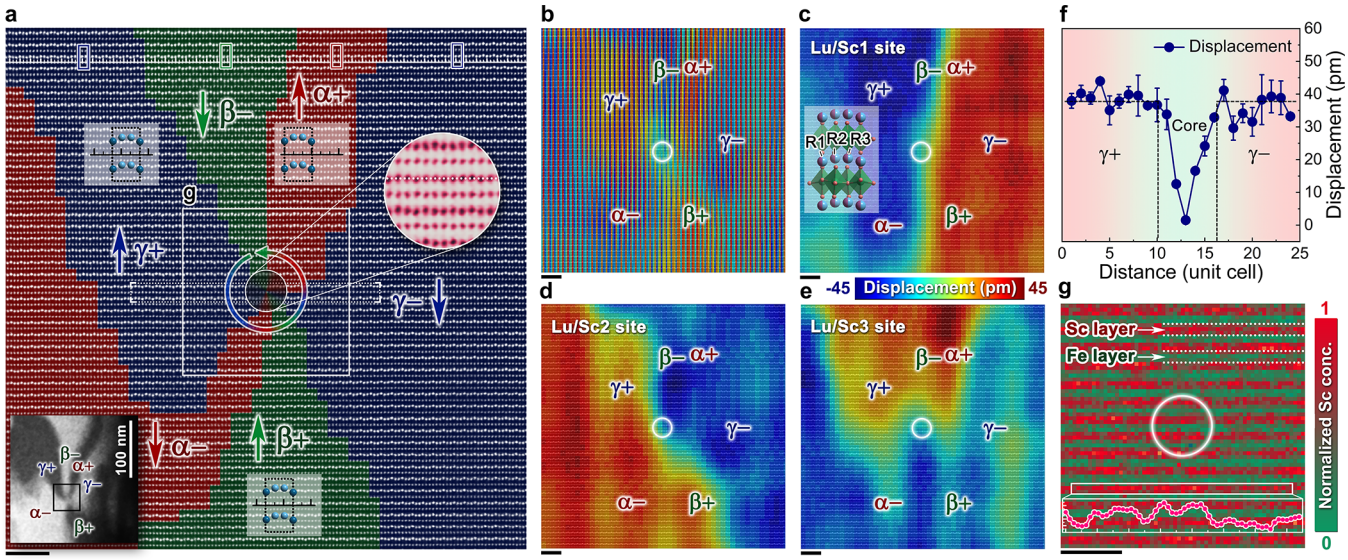

Figure 2. Atomic-scale characterization of an antivortex domain. (a) HAADF-STEM image of a 6-fold antivortex domain, enlarged from the boxed area in the dark-field image at the left bottom corner. Two types of domain walls are identified, labeled as Type-I ($^1/_6$[210]) and Type-II ($^1/_3$[210]) in Figure S4a in the Supporting Information. (b) Displacement color map showing a visible vortex structure with three different Lu/Sc columns (c) Lu/Sc1, (d) Lu/Sc2, and (e) Lu/Sc3. White circles indicate the vortex core. (f) Displacement profile across the vortex core in the dotted-rectangle region in panel (a). (g) Areal concentration map of atomic layer-resolved Sc in the square area in panel (a) with no detectable enrichment or deficiency within the core. Inset is the intensity profile in the white rectangle-framed area, showing the concentration fluctuation. Scale bars = 2 nm.

ferroelectricity via chemical cation substitution, to engineer functional materials.

A nominal h-$Lu_{1-x}Sc_xFeO_3$ ($x \approx 0.51$; see Table S1 in the Supporting Information) single crystal with high phase purity is used for this study. Synthesis details can be found elsewhere.[14] The structural model (Figure 1a, left) was constructed based on the structural refinement from synchrotron X-ray diffraction (SXRD) experiments conducted at BL44B2 in SPring-8 (Figure 1b). Rietveld refinement of X-ray diffractograms in Figure 1b confirms a single hexagonal phase with noncentrosymmetric space group $P6_3cm$ (No. 185), which is consistent with previous studies.[13,19] The atomic structure was characterized using aberration-corrected STEM. Figures 1c–e show high-angle annular dark-field (HAADF)-STEM images at [100], [210], and [001] zone axes, respectively. Since the brightness in HAADF-STEM images is approximatively proportional to $Z^{1.7}$ (where Z is the atomic number),[28] the uniform contrast for Lu/Sc layers (Z_{Sc} = 21 and Z_{Lu} = 71) indicates an average homogeneous distribution of Sc substitutional atoms. As shown in the selected area electron diffraction (SAED) patterns in the right panels of Figures 1c–e, no additional diffraction spots apart from the $P6_3cm$ symmetry can be detected. This means that neither Sc ordering, nor phase separation exists. The symmetry thus changes from orthorhombic to hexagonal upon Sc substitution, reaching a single hexagonal phase. Similar to the hexagonal manganites,[29] the K_3 nonpolar phonon mode ($\mathbf{q} = (^1/_3, ^1/_3, 0)$) condenses in this noncentrosymmetric phase, accompanied by the trimerization of FeO_5 bipyramids that induces corrugated Lu/Sc layers (Figure 1c). Based on Landau theory,[22] there exist six distinct trimerized states, corresponding to six degenerate minima of the lattice energy, that is, six ferroelectric domains that merge to form a vortex (or antivortex) structure. Such a vortex domain structure has been observed at mesoscale using piezoelectric force microscopy (PFM).[19]

To reveal the roles Sc plays in stabilizing the trimerized states, especially the vortex domains, typical vortex domains were imaged and quantitatively analyzed at the atomic scale. Figure 2a shows a HAADF-STEM image of the atomically resolved 6-fold antivortex structure, as well as its corresponding two-beam dark-field image (for an overview of the domain configuration, see Figure S3 in the Supporting Information). The corresponding annular bright-field (ABF) image is shown in Figure S4a in the Supporting Information. Six ferroelectric domains can be distinguished by the up–up–down and up–down–down arrangements of Lu/Sc ions. Following the practice in h-$YMnO_3$,[30] a "lattice ruler" that has the lattice periodicity is added as a reference to identify the transition relationship between domains, as shown at the top of Figure 2a. Since the translational integral lattice periodicity does not change, the domain phases can be determined by comparing the positions of unit cells (marked by rectangles), relative to the short vertical lines in the ruler. In this way, six ferroelectric domains around a core are found to arrange in the sequence of $\alpha^+-\gamma^--\beta^+-\alpha^--\gamma^+-\beta^-$, converging to form an antivortex structure. By conducting a series of quantitative treatments (see the Experimental Methods in the Supporting Information) on Figure 2a, we reveal atomic-scale structural features of this antivortex domain. Figure 2b is the polarization displacement magnitude (δ) map, and the displacement distribution of each R ion at three Lu/Sc columns ($R1$, $R2$, and $R3$) are shown in Figures 2c–e, respectively. The averaged displacement δ of the entire region is determined to be ~41 pm, which is comparable to that of bulk h-$YMnO_3$.[31] In Figures 2c–e, we note that the displacements of the R ions smoothly transmit across domain walls, indicating that the transition regions are several unit cells wide. It is worth mentioning that domain walls may not be viewed edge-on, which may also contribute to their broadening in HAADF-STEM images.[32] Besides, a dramatic reduction of the displacement magnitude is observed within the vortex core (marked by white circles in Figures 2b–

https://doi.org/10.1021/acs.nanolett.1c02123
Nano Lett. XXXX, XXX, XXX−XXX

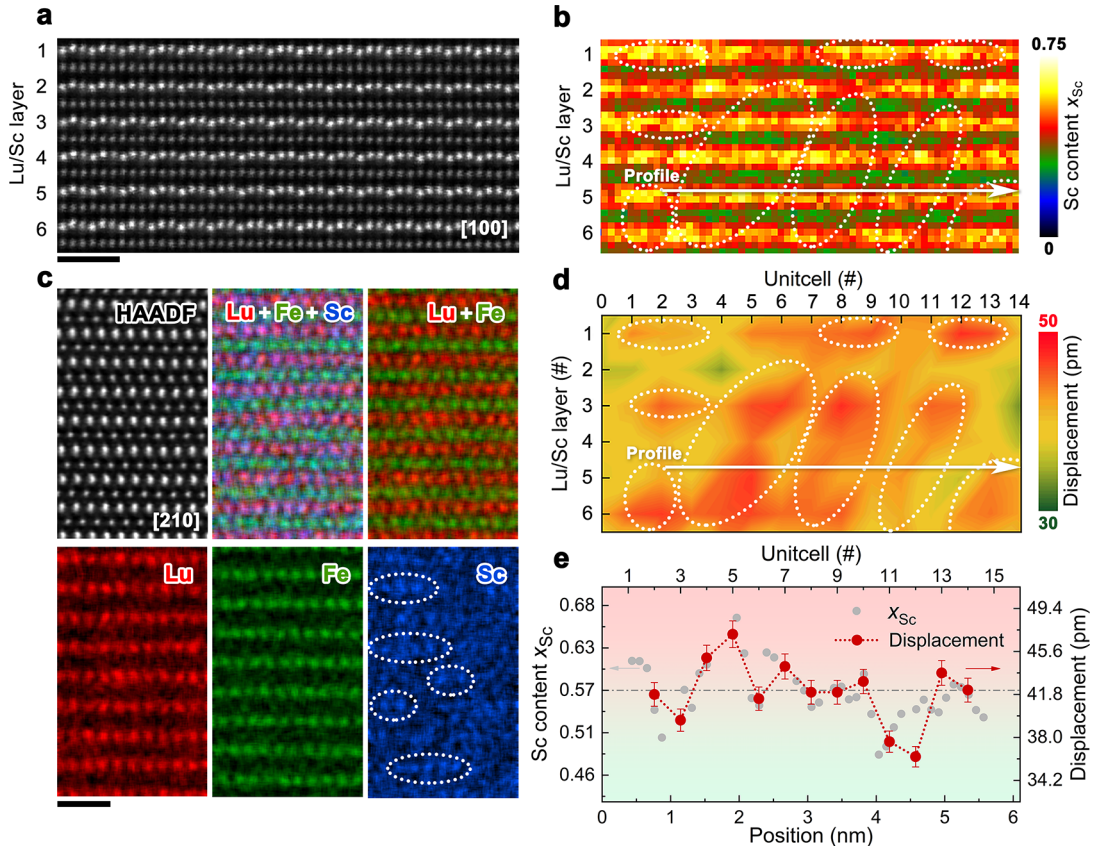

Figure 3. Variation in polar displacement due to fluctuations of Sc concentration. (a) [100] zone axis HAADF-STEM image where the atomically resolved EELS spectrum image was taken. (b) Sc content map of the area in panel (a), showing stoichiometry fluctuations. (c) Atomically resolved EDXS maps. Localized Sc enrichment is circled. (d) Polarization displacement map, showing a clear fluctuation that is consistent with the Sc distributions in panel (b). (e) Profiles along the white arrows in panels (b) and (d), showing the change of Sc content (gray circle) is correlated with the polarization displacement (red circle). Scale bars = 1 nm.

e), which has a radius of ~1 nm. This is consistent with the notable flatness of Lu/Sc layers shown in the close-up (right inset of Figure 2a). Such a displacement drop can be further confirmed by the line profile (Figure 2f) in the dot-framed region in Figure 2a. Therefore, this vortex core shows a significantly decreased magnitude of the primary order parameter (Q_{K3}), which is consistent with a local symmetry of $P\bar{3}c1$ (No. 165) or $P3c1$ (No. 158) symmetry.[33]

The $P\bar{3}c1$ and $P3c1$ phases were shown to have higher energies than the $P6_3cm$ phase and can only exist in regions where strain accumulates and order parameter distributions are not uniform, like at topological defects.[32] Therefore, it is possible that it is energetically favorable for vortex cores to preferentially form at or, be pinned by, regions with higher local Sc content. In our case, since the Sc substitution is directly related to the formation of the vortex domain structure, we conducted an atomic-layer resolved energy-loss spectroscopy (EELS) investigation around the vortex core (square-boxed area in Figure 2a) to examine possible Sc segregation. Figure 2g shows the Sc areal concentration map (see calculation details in the Supporting Information).[34] No evident concentration differences can be found between the areas inside and outside the vortex core, safely excluding the local enrichment of Sc in the core region. However, it is noteworthy that, in each Sc layer, the areal concentration manifests detectable fluctuations, as indicated by the profile in the inset of Figure 2g. Such local concentration fluctuations of Sc that happen within an area much smaller than the typical size of the vortex domain may account for the above-mentioned non-obvious correlation between the vortex core location and Sc distribution. This Sc concentration fluctuation is found to coincide with the variation of the local ferroelectric polarization magnitude in Figure 3.

Figure 3a shows a randomly selected area from an upward polarized domain. The corresponding atomically resolved map of the Sc content (Figure 3b) manifests clear stoichiometry fluctuations. Besides, atomic-resolution elemental maps with energy-dispersive X-ray spectrometry (EDXS) were acquired using the Super-X EDX system. As shown in Figure 3c, strong Lu and Fe signals demonstrate high spatial spectroscopy imaging resolution. For Sc, signals mainly reside within the Lu layers with faint contrast, but importantly, localized intensity variation can be noticed (ellipse-circled regions). To determine how such localized Sc enrichment affects improper ferroelectricity, the corresponding polarization displacement of each unit cell in Figure 3a is calculated in Figure 3d. Unambiguous displacement fluctuations can be observed, which share anomalous characteristics with the Sc content map. Larger (smaller) polarization displacements correspond to higher (lower) Sc concentrations, as indicated in the ellipse-circled areas in Figures 3b and 3d. Further line profiles (Figure 3e) along the white arrows reveal that the variation in displacement magnitude can be correlated with that of the Sc content (for details, see Table S2 and Figure S5 in the Supporting Information). This suggests that the localized enrichment (or deficiency) of Sc can notably increase (or decrease) the local

https://doi.org/10.1021/acs.nanolett.1c02123
Nano Lett. XXXX, XXX, XXX−XXX

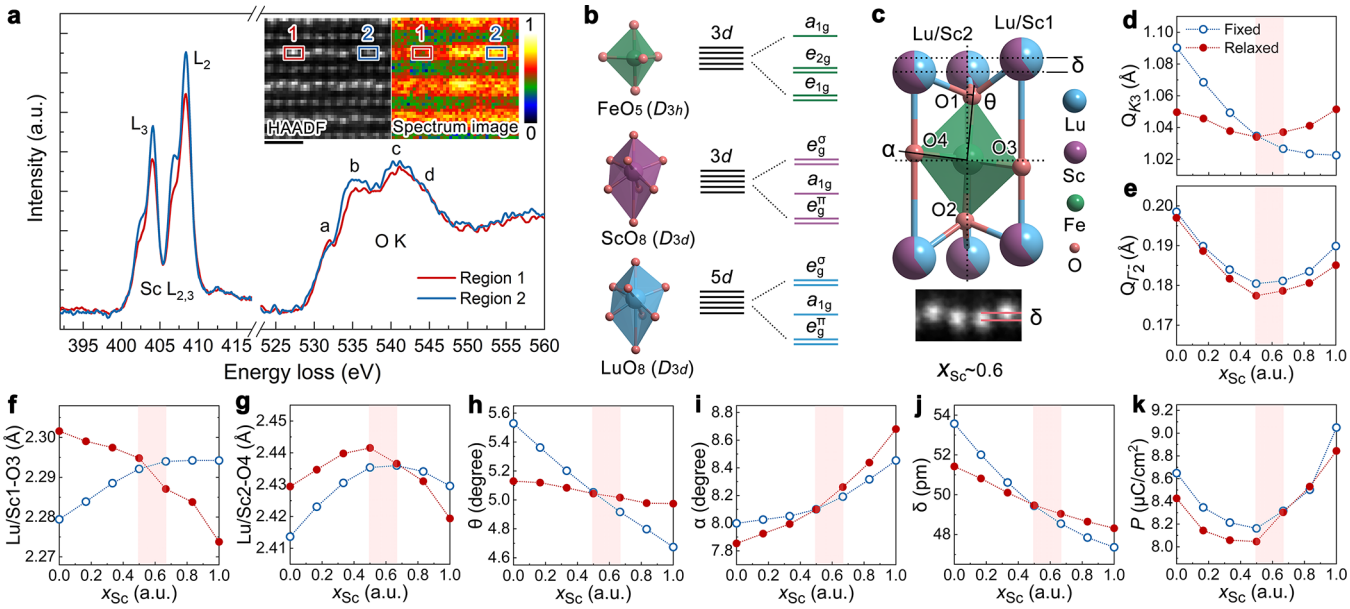

Figure 4. Coupling between the ferroelectric order and Sc content. (a) EELS spectra showing Sc-$L_{2,3}$ and O-K edges from Region-1 and Region-2. Insets are the spectrum image (normalized intensity) and the corresponding HAADF-STEM image. Scale bar = 5 Å. (b) Crystal field splitting for FeO_5 (D_{3h}), ScO_8 (D_{3d}), and LuO_8 (D_{3d}). (c) Schematic illustration of the FeO_5 trimerization. DFT-calculated (d) K_3 mode amplitude (Q_{K3}), (e) Γ_2^- mode amplitude ($Q_{\Gamma_2^-}$), (f) Lu/Sc1−O3 bond length, (g) Lu/Sc2−O4 bond length, (h) apical FeO_5 tilt angle (θ), (i) planar FeO_5 tilt angle (α), (j) Lu/Sc displacements (δ), and (k) polarization (P), as a function of x_{Sc}. Shaded areas indicate the experimental x_{Sc} window.

trimerization magnitude that is associated with the polarization displacement and improper ferroelectricity. We note that measurements at some atomic positions have relatively large error bars, which may be related to the small imperfection of the area that can give rise to changes in inelastic delocalization and probe channeling[35] and/or the random error in measurement. Such effects of substitutional atoms on the trimerization magnitude were recently also demonstrated in cations-doped h-$YMnO_3$ based on theoretical studies, where Zr doping was found to yield a robust ferroelectric state.[36]

The origin of the improper ferroelectricity in hexagonal manganites is still under debate regarding the contribution of the electrostatics and the R−O hybridization.[37−39] Particularly, whether the R−O hybridization plays a part and favors the ferroelectric state is under contention.[38,39] To understand the origin of this close connection between the Sc chemical substitution and improper ferroelectric polarization, we investigated the electronic structures based on EELS near-edge structures. EELS spectra containing Sc-$L_{2,3}$ and O-K edges are plotted in Figure 4a, which are acquired from the corresponding regions in the insets. The high spatial resolution measurement, manifested by the simultaneously pixel-by-pixel acquired HAADF-STEM image, enables the investigations of the local electronic structure. As indicated in the Sc-$L_{2,3}$ spectrum image and the plot, Region-2 has a higher Sc concentration than Region-1. Note that factors other than Sc concentration should be negligible since these two regions are within a pretty small area (~1 nm^2). Such differences in Sc concentration induce different local electronic states, manifested by notable differences in O-K edges that reflect subtle changes in hybridization. Analogous to hexagonal manganites,[38,40] the FeO_5 polyhedron in h-$Lu_{1-x}Sc_xFeO_3$ has D_{3h} site symmetry, where five degenerate Fe 3d orbitals split into two doublets (e_{1g} and e_{2g}) and one singlet (a_{1g}). As for ScO_8 and LuO_8 cages with D_{3d} site symmetry, Sc 3d and Lu 5d orbitals split into three sets: e_g^σ, a_{1g}, and e_g^π (see Figure 4b). Accordingly, four subpeaks (noted as a, b, c, and d) are observed in the O-K edge and can be divided into three hybridization regions (oxygens hybridize with cations), that is, Fe−O and Sc−O region (peak a and peak d), Lu−O and Sc−O region (peak b), and Lu−O and Fe−O region (peak c) (see details in Figure S6 in the Supporting Information). Compared to Region-1 with lower Sc concentration, peak b that is dominated by the Lu/Sc−O hybridization shows apparently increased intensity for Region-2 with higher Sc concentration. This suggests that the Lu/Sc−O hybridization strength is reinforced by the enrichment of Sc. According to Harrison's rule for the p−d hybridization,[41] such an enhanced hybridization strength results from the decreased bond lengths between Lu/Sc and planar oxygen (O_P, that is O3 and O4), which is also confirmed by theoretical calculations (Figures 4f and 4g). Meanwhile, the Fe−O_P hybridization strength is weakened, accounting for the slight intensity drop in peak a.

To provide fundamental insights into the coupling between the ferroelectric properties and Sc content (x_{Sc}), we further performed density functional theory (DFT) calculations on h-$Lu_{1-x}Sc_xFeO_3$ with fixed and relaxed lattice parameters (see the Theoretical Methods in the Supporting Information). DFT results reveal an intricate coupling between x_{Sc} and the ferroelectric order, as apparent from the x_{Sc}-dependent K_3 (corresponds to a collective rotation of FeO_5 bipyramids) and Γ_2^- (corresponds to the $\mathbf{c}$-axial uneven atomic displacement) mode amplitudes (Q_{K3} and $Q_{\Gamma_2^-}$) shown in Figures 4d and 4e, respectively. When the lattice is fixed, Q_{K3} decreases with increasing x_{Sc} (Figure 4d), resulting from the inverse proportionality to Lu/Sc1−O3 bond lengths in Figure 4f. For the relaxed lattice scenario, Q_{K3} exhibits a parabola-like shape, because of the combined Lu/Sc−O_P effect (see Figure S7a in the Supporting Information). The $Q_{\Gamma_2^-}$ mode amplitude (Figure 4e), inversely proportional to the Lu/Sc2−O4 bond length (Figure 4g), is found to be insensitive to either fixing or

https://doi.org/10.1021/acs.nanolett.1c02123
Nano Lett. XXXX, XXX, XXX−XXX

relaxing the lattice, both cases showing a parabola-like shape. Particularly, it is noteworthy that, with the lattice parameters relaxed, both Q_{K3} and $Q_{\Gamma_2^-}$ increase with increasing x_{Sc} in the experimental Sc content window, because of the enhanced Lu/Sc−O_P bond strength (Figures 4f and 4g), which is consistent with experimental observations (Figure 4a). These perturbations in the ferroelectric order are also reflected by changes in the apical (θ) and planar (α) FeO_5 tilt angles, the Lu/Sc displacements (δ), and the polarization (P) in Figures 4h−k. Caused by the shortening of the Lu/Sc−O_A (apical oxygen) bonds (Figure S7b in the Supporting Information), θ decreases with increasing x_{Sc}, as shown in Figure 4h. The increased α with increasing x_{Sc} results from an increased off-centering of the two planar oxygens. The reasoning for the changes in δ is more complex and discussed in detail in Figure S7 in the Supporting Information. Following the trend of the polar Γ_2^- mode amplitude (Figure 4e), P shows a similar parabola shape, as expected, and also exhibits an increase with increasing x_{Sc} in the experimental x_{Sc} window. Moreover, we self-consistently determine how changing the Sc content perturbs the free-energy landscape of polarization switching (see Figure S8 in the Supporting Information).[36] Generally, increasing x_{Sc} results in more shallow energy minima and lower domain switching energy barriers (ΔE). However, interestingly, a small increase in ΔE with increasing x_{Sc} is observed in the experimental x_{Sc} window, indicating a strengthened ferroelectric domain state by Sc substitutional atoms.

It is worth mentioning that certain longer-range local crystal structures and/or electronic effects, such as local strain variation, which, although expected to influence the local ferroelectricity, cannot be well captured in our DFT calculations. In addition, both the Curie temperature[42−44] and the domain structure formation[45] are also dependent on the R-cation. This could lead to local fluctuations in T_C, with the corresponding heterogeneous formation of the ferroelectric state when cooling across T_C, which, in turn, could affect the resulting local R-cation displacements. Such effects could be investigated further using, e.g., large-scale DFT calculations[33] or phenomenological modeling.[46] Nevertheless, our theoretical assessment further underlines the key roles that Sc atoms play in determining improper ferroelectricity of the h-$Lu_{1-x}Sc_xFeO_3$ system by small perturbations of the local atomic and electronic structure, consistent with experimental results. On this base, the strong dependence of improper ferroelectricity on Sc substitutional atoms is readily established regarding both their distribution and concentration.

In summary, based on elaborate electron microscopy and theoretical studies, we reveal the atomic structure of the intriguing vortex domain stabilized by Sc substitution in multiferroic h-$Lu_{1-x}Sc_xFeO_3$ and clarify the critical roles of individual Sc atoms in controlling its ferroelectricity. By directly mapping the distributions of Sc atoms at the atomic scale, concentration fluctuations are observed, which manifest a close correlation with the variation of improper ferroelectric polarization. We show that Sc substitutional atoms locally modify the atomic and electronic structure, resulting in a tuning of the trimerization magnitude and Lu/Sc−O hybridization strength, which determines the essence of improper ferroelectricity. This is also corroborated by systematic first-principles calculations. The effects of Sc substitution are thus established on the atomic scale, and the insights point to an effective way to tune improper ferroelectrics and understand their underlying mechanism. By directly correlating atomic-scale local structures regulated by individual foreign atoms with global properties, the approach of this study is widely applicable to numerous chemically doped or substituted functional materials to understand and boost their emergent functionalities.

■ ASSOCIATED CONTENT

Supporting Information

The Supporting Information is available free of charge at https://pubs.acs.org/doi/10.1021/acs.nanolett.1c02123.

Details for experimental methods for the single crystal growth, TEM sample preparation, electron microscopy investigations, quantitative analysis of polarization displacement, and quantitative analysis of Sc content; theoretical methods for calculating the ferroelectric orders; supplementary tables for the quantitative analysis of Sc content; and supplementary Figures S1−S10 (PDF)

■ AUTHOR INFORMATION

Corresponding Authors

Shiqing Deng − *School of Mathematics and Physics, University of Science and Technology Beijing, Beijing 100083, China; School of Materials Science and Engineering, Tsinghua University, Beijing 100084, China; Condensed Matter Physics and Materials Science Department, Brookhaven National Laboratory, Upton, New York 11973, United States;* orcid.org/0000-0001-7016-4084; Email: sqdeng@ustb.edu.cn

Yimei Zhu − *Condensed Matter Physics and Materials Science Department, Brookhaven National Laboratory, Upton, New York 11973, United States;* orcid.org/0000-0002-1638-7217; Email: zhu@bnl.gov

Jing Zhu − *School of Materials Science and Engineering, Tsinghua University, Beijing 100084, China;* orcid.org/0000-0002-2175-9476; Email: jzhu@mail.tsinghua.edu.cn

Authors

Jun Li − *Beijing National Laboratory for Condensed Matter Physics, Institute of Physics, Chinese Academy of Sciences, Beijing 100190, China*

Didrik R. Småbråten − *Department of Chemistry, Biochemistry and Pharmaceutical Sciences, University of Bern, 3012 Bern, Switzerland;* orcid.org/0000-0002-7155-7178

Shoudong Shen − *State Key Laboratory of Surface Physics and Department of Physics, Fudan University, Shanghai 200433, China*

Wenbin Wang − *Institute for Nanoelectronic Devices and Quantum Computing, Fudan University, Shanghai 200433, China*

Jun Zhao − *State Key Laboratory of Surface Physics and Department of Physics, Fudan University, Shanghai 200433, China*

Jing Tao − *Condensed Matter Physics and Materials Science Department, Brookhaven National Laboratory, Upton, New York 11973, United States*

Ulrich Aschauer − *Department of Chemistry, Biochemistry and Pharmaceutical Sciences, University of Bern, 3012 Bern, Switzerland;* orcid.org/0000-0002-1165-6377

https://doi.org/10.1021/acs.nanolett.1c02123
Nano Lett. XXXX, XXX, XXX−XXX

Jun Chen − *School of Mathematics and Physics, University of Science and Technology Beijing, Beijing 100083, China;* orcid.org/0000-0002-7330-8976

Complete contact information is available at: https://pubs.acs.org/10.1021/acs.nanolett.1c02123

Author Contributions

S.D., J.Z., and Y.Z. conceived the idea and initiated the research; J.Z., Y.Z., and J.C. supervised the project; S.D. and J.L. performed the STEM characterizations and quantitative analysis; D.R.S. and U.A. conducted theoretical calculations and analysis. The single-crystal samples were grown and provided by S.S., W.W., and J.Z.; S.D., J.L., and D.R.S. performed the data analysis and wrote the manuscript, with help from J.Z., Y.Z., J.C., and J.T.. All authors discussed the results, commented on the manuscript, and have given approval to the final version of the manuscript.

Author Contributions

$^{\nabla}$These authors contributed equally.

Notes

The authors declare no competing financial interest.

■ ACKNOWLEDGMENTS

The electronic microscopy work was performed at Tsinghua University and Brookhaven National Laboratory. The research at Brookhaven National Laboratory was supported by the U.S. DOE Basic Energy Sciences, Materials Sciences and Engineering Division, under Contract No. DESC0012704. J.Z. and S.D. would like to acknowledge the financial support by the National Natural Science Foundation of China (Nos. 51788104 and 11834009). S.D. would like to acknowledge the financial support by the National Natural Science Foundation of China (No. 22001014), the China National Postdoctoral Program for Innovative Talents (No. BX20200043), the China Postdoctoral Science Foundation (No. 2021M690366), and the Fundamental Research Funds for the Central Universities, China (No. 06500145). The research at Fudan University was supported by the Innovation Program of Shanghai Municipal Education Commission (No. 2017-01-07-00-07-E00018), the National Key R&D Program of China (Nos. 2016YFA0300702 and 2016YFA0300203), and the Shanghai Municipal Natural Science Foundation (No. 18JC1411400). Synchrotron X-ray diffraction experiments were performed at BL02B2, BL04B2, and BL44B2 of SPring-8 with approval of the Japan Synchrotron Radiation Research Institute (Proposal Nos. 2019A1167, 2019A1095, 2019A1340, and 2019B1120). D.R.S. and U.A. would like to acknowledge the Swiss National Science Foundation (No. 200021_178791) for financial support. Density functional theory (DFT) calculations were performed on UBELIX (http://www.id.unibe.ch/hpc), the HPC cluster at the University of Bern.

■ REFERENCES

(1) Goodwin, A. L. Opportunities and challenges in understanding complex functional materials. *Nat. Commun.* **2019**, *10* (1), 4461.

(2) Krogstad, M. J.; Gehring, P. M.; Rosenkranz, S.; Osborn, R.; Ye, F.; Liu, Y.; Ruff, J. P. C.; Chen, W.; Wozniak, J. M.; Luo, H.; Chmaissem, O.; Ye, Z. G.; Phelan, D. The relation of local order to material properties in relaxor ferroelectrics. *Nat. Mater.* **2018**, *17* (8), 718−724.

(3) Kumar, A.; Baker, J. N.; Bowes, P. C.; Cabral, M. J.; Zhang, S.; Dickey, E. C.; Irving, D. L.; LeBeau, J. M. Atomic-resolution electron microscopy of nanoscale local structure in lead-based relaxor ferroelectrics. *Nat. Mater.* **2021**, *20* (1), 62−67.

(4) Deng, S.; Wu, L.; Cheng, H.; Zheng, J.-C.; Cheng, S.; Li, J.; Wang, W.; Shen, J.; Tao, J.; Zhu, J.; Zhu, Y. Charge-lattice coupling in hole-doped $LuFe_2O_{4+\delta}$: the origin of second-order modulation. *Phys. Rev. Lett.* **2019**, *122* (12), 126401.

(5) Randall, C. A.; Bhalla, A. S. Nanostructural-property relations in complex lead perovskites. *Jpn. J. Appl. Phys.* **1990**, *29* (2R), 327−333.

(6) Goossens, D. J. Local ordering in lead-based relaxor ferroelectrics. *Acc. Chem. Res.* **2013**, *46* (11), 2597−2606.

(7) Li, F.; Cabral, M. J.; Xu, B.; Cheng, Z.; Dickey, E. C.; LeBeau, J. M.; Wang, J.; Luo, J.; Taylor, S.; Hackenberger, W.; Bellaiche, L.; Xu, Z.; Chen, L.-Q.; Shrout, T. R.; Zhang, S. Giant piezoelectricity of Sm-doped $Pb(Mg_{1/3}Nb_{2/3})O_3$−$PbTiO_3$ single crystals. *Science* **2019**, *364* (6437), 264−268.

(8) Cheong, S.-W.; Mostovoy, M. Multiferroics: a magnetic twist for ferroelectricity. *Nat. Mater.* **2007**, *6* (1), 13−20.

(9) Spaldin, N. A.; Ramesh, R. Advances in magnetoelectric multiferroics. *Nat. Mater.* **2019**, *18* (3), 203−212.

(10) Yang, C. H.; Seidel, J.; Kim, S. Y.; Rossen, P. B.; Yu, P.; Gajek, M.; Chu, Y. H.; Martin, L. W.; Holcomb, M. B.; He, Q.; Maksymovych, P.; Balke, N.; Kalinin, S. V.; Baddorf, A. P.; Basu, S. R.; Scullin, M. L.; Ramesh, R. Electric modulation of conduction in multiferroic Ca-doped $BiFeO_3$ films. *Nat. Mater.* **2009**, *8* (6), 485−493.

(11) Seidel, J.; Maksymovych, P.; Batra, Y.; Katan, A.; Yang, S. Y.; He, Q.; Baddorf, A. P.; Kalinin, S. V.; Yang, C. H.; Yang, J. C.; Chu, Y. H.; Salje, E. K.; Wormeester, H.; Salmeron, M.; Ramesh, R. Domain wall conductivity in La-doped $BiFeO_3$. *Phys. Rev. Lett.* **2010**, *105* (19), 197603.

(12) Disseler, S. M.; Luo, X.; Gao, B.; Oh, Y. S.; Hu, R.; Wang, Y.; Quintana, D.; Zhang, A.; Huang, Q.; Lau, J.; Paul, R.; Lynn, J. W.; Cheong, S.-W.; Ratcliff, W. Multiferroicity in doped hexagonal $LuFeO_3$. *Phys. Rev. B: Condens. Matter Mater. Phys.* **2015**, *92* (5), 054435.

(13) Masuno, A.; Ishimoto, A.; Moriyoshi, C.; Hayashi, N.; Kawaji, H.; Kuroiwa, Y.; Inoue, H. Weak ferromagnetic transition with a dielectric anomaly in hexagonal $Lu_{0.5}Sc_{0.5}FeO_3$. *Inorg. Chem.* **2013**, *52* (20), 11889−11894.

(14) Lin, L.; Zhang, H. M.; Liu, M. F.; Shen, S.; Zhou, S.; Li, D.; Wang, X.; Yan, Z. B.; Zhang, Z. D.; Zhao, J.; Dong, S.; Liu, J.-M. Hexagonal phase stabilization and magnetic orders of multiferroic $Lu_{1-x}Sc_xFeO_3$. *Phys. Rev. B: Condens. Matter Mater. Phys.* **2016**, *93* (7), 075146.

(15) Disseler, S. M.; Borchers, J. A.; Brooks, C. M.; Mundy, J. A.; Moyer, J. A.; Hillsberry, D. A.; Thies, E. L.; Tenne, D. A.; Heron, J.; Holtz, M. E.; Clarkson, J. D.; Stiehl, G. M.; Schiffer, P.; Muller, D. A.; Schlom, D. G.; Ratcliff, W. D. Magnetic structure and ordering of multiferroic hexagonal $LuFeO_3$. *Phys. Rev. Lett.* **2015**, *114* (21), 217602.

(16) Das, H.; Wysocki, A. L.; Geng, Y.; Wu, W.; Fennie, C. J. Bulk magnetoelectricity in the hexagonal manganites and ferrites. *Nat. Commun.* **2014**, *5* (1), 2998.

(17) Fabréges, X.; Petit, S.; Mirebeau, I.; Pailhes, S.; Pinsard, L.; Forget, A.; Fernandez-Diaz, M. T.; Porcher, F. Spin-lattice coupling, frustration, and magnetic order in multiferroic $RMnO_3$. *Phys. Rev. Lett.* **2009**, *103* (6), 067204.

(18) Katsufuji, T.; Mori, S.; Masaki, M.; Moritomo, Y.; Yamamoto, N.; Takagi, H. Dielectric and magnetic anomalies and spin frustration in hexagonal $RMnO_3$ (R = Y, Yb, and Lu). *Phys. Rev. B: Condens. Matter Mater. Phys.* **2001**, *64* (10), 104419.

(19) Du, K.; Gao, B.; Wang, Y.; Xu, X.; Kim, J.; Hu, R.; Huang, F.-T.; Cheong, S.-W. Vortex ferroelectric domains, large-loop weak ferromagnetic domains, and their decoupling in hexagonal (Lu, Sc)FeO_3. *npj Quantum Mater.* **2018**, *3* (1), 33.

(20) Fiebig, M.; Lottermoser, T.; Fröhlich, D.; Goltsev, A. V.; Pisarev, R. V. Observation of coupled magnetic and electric domains. *Nature* **2002**, *419* (6909), 818−820.

(21) Geng, Y.; Lee, N.; Choi, Y. J.; Cheong, S.-W.; Wu, W. Collective magnetism at multiferroic vortex domain walls. *Nano Lett.* **2012**, *12* (12), 6055−6059.
(22) Artyukhin, S.; Delaney, K. T.; Spaldin, N. A.; Mostovoy, M. Landau theory of topological defects in multiferroic hexagonal manganites. *Nat. Mater.* **2014**, *13* (1), 42−49.
(23) Mundy, J. A.; Schaab, J.; Kumagai, Y.; Cano, A.; Stengel, M.; Krug, I. P.; Gottlob, D. M.; Dog Anay, H.; Holtz, M. E.; Held, R.; Yan, Z.; Bourret, E.; Schneider, C. M.; Schlom, D. G.; Muller, D. A.; Ramesh, R.; Spaldin, N. A.; Meier, D. Functional electronic inversion layers at ferroelectric domain walls. *Nat. Mater.* **2017**, *16* (6), 622−627.
(24) Kawamoto, T.; Fujita, K.; Yamada, I.; Matoba, T.; Kim, S. J.; Gao, P.; Pan, X.; Findlay, S. D.; Tassel, C.; Kageyama, H.; Studer, A. J.; Hester, J.; Irifune, T.; Akamatsu, H.; Tanaka, K. Room-temperature polar ferromagnet $ScFeO_3$ transformed from a high-pressure orthorhombic perovskite phase. *J. Am. Chem. Soc.* **2014**, *136* (43), 15291−15299.
(25) Li, M. R.; Adem, U.; McMitchell, S. R.; Xu, Z.; Thomas, C. I.; Warren, J. E.; Giap, D. V.; Niu, H.; Wan, X.; Palgrave, R. G.; Schiffmann, F.; Cora, F.; Slater, B.; Burnett, T. L.; Cain, M. G.; Abakumov, A. M.; van Tendeloo, G.; Thomas, M. F.; Rosseinsky, M. J.; Claridge, J. B. A polar corundum oxide displaying weak ferromagnetism at room temperature. *J. Am. Chem. Soc.* **2012**, *134* (8), 3737−3747.
(26) Zhu, W.; Pi, L.; Tan, S.; Zhang, Y. Anisotropy and extremely high coercivity in weak ferromagnetic $LuFeO_3$. *Appl. Phys. Lett.* **2012**, *100* (5), 052407.
(27) Masuno, A.; Ishimoto, A.; Moriyoshi, C.; Kawaji, H.; Kuroiwa, Y.; Inoue, H. Expansion of the hexagonal phase-forming region of $Lu_{1-x}Sc_xFeO_3$ by containerless processing. *Inorg. Chem.* **2015**, *54* (19), 9432−9437.
(28) Pennycook, S. J.; Jesson, D. E. High-resolution *Z*-contrast imaging of crystals. *Ultramicroscopy* **1991**, *37* (1−4), 14−38.
(29) Fennie, C. J.; Rabe, K. M. Ferroelectric transition in $YMnO_3$ from first principles. *Phys. Rev. B: Condens. Matter Mater. Phys.* **2005**, *72* (10), 100103.
(30) Zhang, Q.; Tan, G.; Gu, L.; Yao, Y.; Jin, C.; Wang, Y.; Duan, X.; Yu, R. Direct observation of multiferroic vortex domains in $YMnO_3$. *Sci. Rep.* **2013**, *3* (1), 2741.
(31) Deng, S.; Cheng, S.; Xu, C.; Ge, B.; Sun, X.; Yu, R.; Duan, W.; Zhu, J. Atomic mechanism of hybridization-dependent surface reconstruction with tailored functionality in hexagonal multiferroics. *ACS Appl. Mater. Interfaces* **2017**, *9* (32), 27322−27331.
(32) Li, J.; Chiang, F. K.; Chen, Z.; Ma, C.; Chu, M. W.; Chen, C. H.; Tian, H.; Yang, H.; Li, J. Homotopy-theoretic study & atomic-scale observation of vortex domains in hexagonal manganites. *Sci. Rep.* **2016**, *6* (1), 28047.
(33) Småbråten, D. R.; Nakata, A.; Meier, D.; Miyazaki, T.; Selbach, S. M. First-principles study of topologically protected vortices and ferroelectric domain walls in hexagonal $YGaO_3$. *Phys. Rev. B: Condens. Matter Mater. Phys.* **2020**, *102* (14), 144103.
(34) Egerton, R. F. *Electron Energy-Loss Spectroscopy in the Electron Microscope*, 3rd Edition; Springer Science+Business Media: New York, 2011.
(35) Allen, L. J.; Findlay, S. D.; Oxley, M. P.; Witte, C.; Zaluzec, N. J. Modelling high-resolution electron microscopy based on core-loss spectroscopy. *Ultramicroscopy* **2006**, *106* (11−12), 1001−1011.
(36) Småbråten, D. R.; Holstad, T. S.; Evans, D. M.; Yan, Z.; Bourret, E.; Meier, D.; Selbach, S. M. Domain wall mobility and roughening in doped ferroelectric hexagonal manganites. *Phys. Rev. Res.* **2020**, *2* (3), 033159.
(37) Van Aken, B. B.; Palstra, T. T.; Filippetti, A.; Spaldin, N. A. The origin of ferroelectricity in magnetoelectric $YMnO_3$. *Nat. Mater.* **2004**, *3* (3), 164−170.
(38) Cho, D. Y.; Kim, J. Y.; Park, B. G.; Rho, K. J.; Park, J. H.; Noh, H. J.; Kim, B. J.; Oh, S. J.; Park, H. M.; Ahn, J. S.; Ishibashi, H.; Cheong, S.-W.; Lee, J. H.; Murugavel, P.; Noh, T. W.; Tanaka, A.; Jo, T. Ferroelectricity driven by Y d^0-ness with rehybridization in $YMnO_3$. *Phys. Rev. Lett.* **2007**, *98* (21), 217601.
(39) Kumagai, Y.; Belik, A. A.; Lilienblum, M.; Leo, N.; Fiebig, M.; Spaldin, N. A. Observation of persistent centrosymmetricity in the hexagonal Manganite family. *Phys. Rev. B: Condens. Matter Mater. Phys.* **2012**, *85* (17), 174422.
(40) Cheng, S.; Li, M.; Meng, Q.; Duan, W.; Zhao, Y. G.; Sun, X. F.; Zhu, Y.; Zhu, J. Electronic and crystal structure changes induced by in-plane oxygen vacancies in multiferroic $YMnO_3$. *Phys. Rev. B: Condens. Matter Mater. Phys.* **2016**, *93* (5), 054409.
(41) Harrison, W. A. *Electronic Structure and the Properties of Solids*; W. H. Freeman and Co.: San Francisco, CA, 1980.
(42) Gibbs, A. S.; Knight, K. S.; Lightfoot, P. High-temperature phase transitions of hexagonal $YMnO_3$. *Phys. Rev. B: Condens. Matter Mater. Phys.* **2011**, *83* (9), 094111.
(43) Lilienblum, M.; Lottermoser, T.; Manz, S.; Selbach, S. M.; Cano, A.; Fiebig, M. Ferroelectricity in the multiferroic hexagonal manganites. *Nat. Phys.* **2015**, *11* (12), 1070−1073.
(44) Evans, D. M.; Garcia, V.; Meier, D.; Bibes, M. Domains and domain walls in multiferroics. *Phys. Sci. Rev.* **2020**, *5* (9), 20190067.
(45) Meier, Q. N.; Lilienblum, M.; Griffin, S. M.; Conder, K.; Pomjakushina, E.; Yan, Z.; Bourret, E.; Meier, D.; Lichtenberg, F.; Salje, E. K. H.; Spaldin, N. A.; Fiebig, M.; Cano, A. Global formation of topological defects in the multiferroic hexagonal manganites. *Phys. Rev. X* **2017**, *7* (4), 041014.
(46) Lin, H. L.; Yang, K. L.; Chen, P. Z.; Zhou, G. Z.; Li, C. F.; Zheng, S. H.; Lin, L.; Yan, Z. B.; Jiang, X. P.; Liu, J.-M. Suppression of vortex-antivortex structures by anti-trimer point defects in hexagonal manganites. *J. Appl. Phys.* **2020**, *127* (19), 194106.

https://doi.org/10.1021/acs.nanolett.1c02123
Nano Lett. XXXX, XXX, XXX−XXX